Binding Motif of Terminal Alkynes on Gold Clusters

ARTICLE *in* JOURNAL OF THE AMERICAN CHEMICAL SOCIETY · MAY 2013

Impact Factor: 12.11 · DOI: 10.1021/ja401798z · Source: PubMed

5 AUTHORS, INCLUDING:

Prasenjit Maity
Gujarat Forensic Sciences University
16 PUBLICATIONS **348** CITATIONS

SEE PROFILE

JACS
JOURNAL OF THE AMERICAN CHEMICAL SOCIETY

Article

pubs.acs.org/JACS

Binding Motif of Terminal Alkynes on Gold Clusters

Prasenjit Maity,[†] Shinjiro Takano,[†] Seiji Yamazoe,[†,‡] Tomonari Wakabayashi,[§] and Tatsuya Tsukuda*[,†,‡]

[†]Department of Chemistry, School of Science, The University of Tokyo, 7-3-1 Hongo, Bunkyo-ku, Tokyo 113-0033, Japan
[‡]Elements Strategy Initiative for Catalysts and Batteries (ESICB), Kyoto University, Katsura, Kyoto 615-8520, Japan
[§]Department of Chemistry, School of Science and Engineering, Kinki University, Higashiosaka, Osaka 577-8502, Japan

Supporting Information

ABSTRACT: Gold clusters protected by terminal alkynes (1-octyne (OC-H), phenylacetylene (PA-H) and 9-ethynyl-phenanthrene (EPT-H)) were prepared by the ligand exchange of small (diameter <2 nm) Au clusters stabilized by polyvinylpyrrolidone. The bonding motif of these alkynes on Au clusters was investigated using various spectroscopic methods. FTIR and Raman spectroscopy revealed that terminal hydrogen is lost during the ligand exchange and that the C≡C bond of the alkynyl group is weakened upon attachment to the Au clusters. Acidification of the water phase after the ligand exchange indicated that the ligation of alkynyl groups to the Au clusters proceeds via deprotonation of the alkynes. A series of precisely defined Au clusters, $Au_{34}(PA)_{16}$, $Au_{54}(PA)_{26}$, $Au_{30}(EPT)_{13}$, $Au_{35}(EPT)_{18}$, and $Au_{41-43}(EPT)_{21-23}$, were synthesized and characterized in detail to obtain further insight into the interfacial structures. Careful mass analysis confirmed the ligation of the alkynes in the dehydrogenated form. An upright configuration of the alkynes on Au clusters was suggested from the Au to alkyne ratios and photoluminescence from the excimer of the EPT ligands. EXAFS analysis implied that the alkynyl carbon is bound to bridged or hollow sites on the cluster surface.

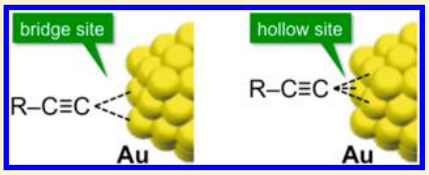

INTRODUCTION

Gold clusters protected by organic ligands (phosphines and thiolates) have gained much recent attention as a prototypical system for fundamental studies as well as nanoscale building units of novel functional materials.[1−10] The previous studies have revealed that their properties and functionalities are governed by three structure parameters: (1) the number of Au atoms in the core (core size), (2) the interfacial structure between the Au core and the ligands, and (3) the functionalities of the tail groups of the ligands. First, state-of-the-art synthesis has allowed us to obtain a series of stable Au clusters with well-defined core sizes, although universal control of any desired size remains a challenge. Second, the geometric and electronic structures at the interface depend strongly on the nature of the head groups of the ligands. X-ray crystallography revealed that phosphines are coordinated atop sites of the Au core,[1,11−13] whereas thiolates (RS) form −SR−[Au−SR−]$_n$ oligomers that are coordinated in a bidentate fashion atop sites of the Au core.[4−10,14] Although rare, the binding of monomeric thiolates on bridged sites of the Au core has been found in $Au_{11}(SR)_3(PPh_3)_7$,[15] $[Au_{25}(SR)_5(PPh_3)_{10}Cl_2]^{2+}$,[16] and $Au_{36}(SR)_{24}$.[17] Recently, we proposed that bulky arenethiols (Eind-S) are individually bonded to a putative Au_{41} core of a twisted-pyramidal structure without forming Au−thiolate oligomers in $Au_{41}(S\text{-Eind})_{12}$.[18] The electronic charge transferred at the Au−phosphine interface is negligibly small, whereas each of the thiolates formally takes one valence electron from the Au core.[19] Third, one can furnish a variety of tailor-made functions by proper design and chemical synthesis of the ligands.[20]

Recently, terminal alkynes (RC≡CH) have come into use as a new type of protective ligand of Au clusters/nanoparticles.[21−25] We reported the first synthesis of phenylacetylene-protected Au clusters (Au:PA) by using a biphasic ligand exchange of preformed polyvinylpyrrolidone (PVP)-stabilized Au clusters (diameter <2 nm).[26] We also succeeded in synthesizing a magic cluster, $Au_{54}(PA)_{26}$, selectively under specific optimized reaction conditions.[27] One can expect that this class of *organogold clusters* will exhibit novel photophysical and electronic properties because of intimate coupling between the tail group of the ligands and Au clusters via Au−C covalent bonds. In fact, Wandlowski has demonstrated that electronic conductance of a single dialkyne molecule between two Au electrodes is much higher than that of dithiols or other traditional molecules.[28] Delocalization of electronic charge over alkyne-protected Ru clusters has been reported by Chen.[29] However, fundamental information about the interfacial structures between the terminal alkynes and Au clusters and their formation process is still lacking.

Four types of binding motifs of terminal alkynes have been proposed on Au surfaces and nanoparticles as shown in Scheme 1.[23,29−36] In type 1, the alkynyl group (RC≡C−) formed by dehydrogenation of the alkyne is bonded to the Au surface in an upright configuration via a σ interaction.[23,30−33] Adsorption of RC≡C− on atop,[31] bridged,[32] or hollow sites[33] of Au surfaces has been proposed. This type of binding was also produced by the reaction of ruthenium (Ru) nanoparticles and 1-octynyllithium.[29,37] In type 2, the alkynyl group (RC≡C−) is

Received: February 23, 2013
Published: May 31, 2013

   dx.doi.org/10.1021/ja401798z | J. Am. Chem. Soc. 2013, 135, 9450−9457

Scheme 1. Proposed Binding Motifs of Alkynes to a Au Surface and a Au Nanoparticle

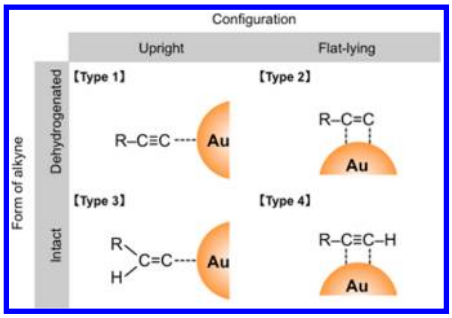

bonded in a flat-lying configuration to the Au surface via a $\sigma-\pi$ interaction.[34,35] In type 3, the vinylidene group (RCH═C═) formed by intramolecular hydrogen transfer is bonded in an upright configuration.[33] This type of binding has been proposed between 1-dodecyne and Ru nanoparticles.[38] In type 4, the intact alkyne is bonded in a flat-lying configuration to the Au surface via a π interaction.[36] An understanding of the binding motif will not only help establish structure−function correlations of alkyne-protected Au clusters but will also provide useful information for the development of Au-based catalysts for reactions which involve alkyne activation (for example, Sonogashira coupling, hydrogenation, hydration, and hydrosilylation)[39−44] and nanoscale electronic devices based on the Au−C interface.[28]

The present work aims to elucidate the interfacial structures between small Au clusters and selected terminal alkynes: 1-octyne (OC-H), phenylacetylene (PA-H), and 9-ethynylphenanthrene (EPT-H). Since a straightforward approach by single-crystal X-ray crystallography is not currently available, we tackled the issue by combining various spectroscopic techniques, including vibrational spectroscopy, mass spectrometry, fluorescent spectroscopy, and extended X-ray absorption fine structure (EXAFS) analysis. A series of clusters with well-defined compositions, $Au_{54}(PA)_{26}$, $Au_{34}(PA)_{16}$, $Au_{41-43}(EPT)_{21-23}$, $Au_{35}(EPT)_{18}$, and $Au_{30}(EPT)_{13}$, were synthesized and used for in-depth examination of the interfacial structures. Loss of terminal hydrogen was confirmed by IR spectroscopy and mass spectrometry. Chemical compositions and photoluminescence (PL) behavior of the chromophoric sites indicated an upright configuration of the alkynyl ligands via a Au−C covalent bond. The EXAFS data suggested that the carbon is bonded to bridged and/or hollow sites of the Au atoms. The mechanism of bond formation of the terminal alkynes on Au clusters is discussed on the basis of the results.

RESULTS AND DISCUSSION

Characterization of As-Prepared Clusters. As reported previously, alkyne-protected Au clusters could not be obtained by reduction of $AuCl_4^-$ in the presence of alkynes.[45] Thus, a biphasic ligand exchange protocol was developed for their synthesis (Scheme 2).[26,27] Briefly, PVP-stabilized Au clusters with an average diameter of 1.2 ± 0.2 nm, Au:PVP(**1**) (Figure S1, Supporting Information),[46] were prepared by microfluidic mixing of the aqueous solutions of $HAuCl_4$/PVP (15 mL) and $NaBH_4$/PVP (15 mL). Then, an aqueous solution of Au:PVP(**1**) was mixed with a chloroform solution of the alkyne (OC-H, PA-H, or EPT-H) at 333 K with vigorous stirring for 2 h. The alkyne-protected Au clusters thus produced from Au:PVP(**1**) will be referred to hereafter as Au:OC, Au:PA,

Scheme 2. Synthesis of Alkyne-Protected Au Clusters

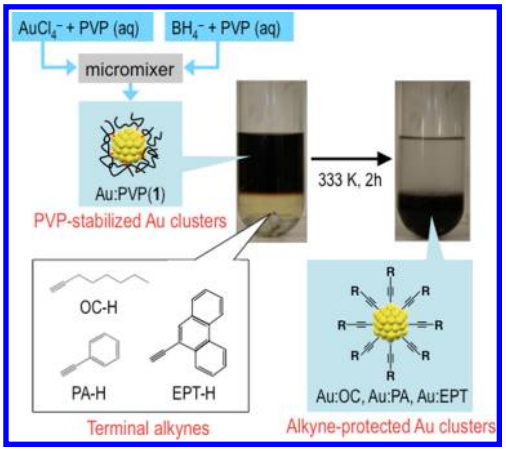

and Au:EPT, respectively. It should be noted that Au:PVP clusters larger than 4 nm did not form alkyne-protected clusters via ligand exchange, implying that the ligation is based on the size-specific reactivity of the Au:PVP clusters.

The average diameters of Au:OC, Au:PA, and Au:EPT were determined to be 3.2 ± 0.8, 1.4 ± 0.2, and 1.4 ± 0.2 nm, respectively, by analyzing TEM images of more than 300 particles (Figure 1). The surface plasmon band in the optical

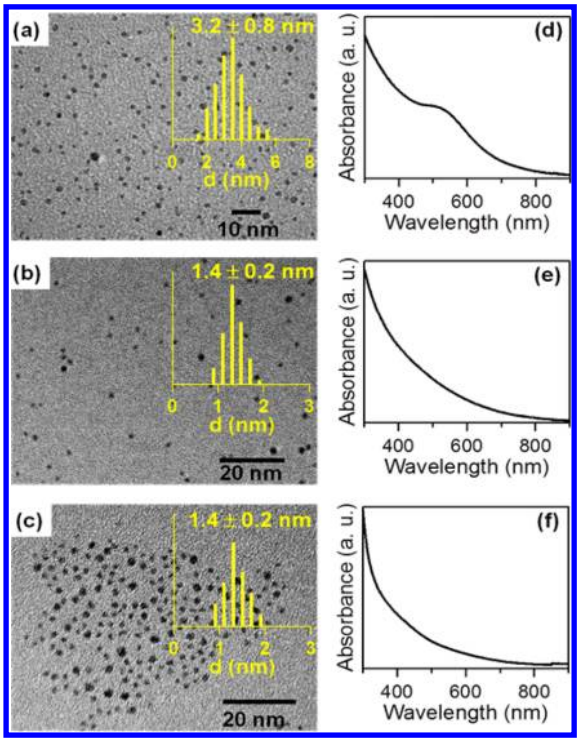

Figure 1. TEM images and particle size histograms of as-prepared (a) Au:OC, (b) Au:PA, and (c) Au:EPT and UV−vis spectra of (d) Au:OC, (e) Au:PA, and (f) Au:EPT.

absorption spectra in Figure 1d indicates that the diameter of Au:OC is larger than those of the others. The larger size of Au:OC in comparison to Au:PA and Au:EPT is ascribed to its instability to aggregation in solution. In contrast, Au:PA and Au:EPT were stable and did not show any noticeable degradation over a few days. After storage in chloroform at 273 K for 6 months, it was found that Au:PA clusters were

dx.doi.org/10.1021/ja401798z | J. Am. Chem. Soc. 2013, 135, 9450−9457

transformed into larger particles with an average diameter of 20 ± 4 nm (Figure S2, Supporting Information).[46] In contrast, TEM and UV−vis optical spectroscopy indicated that Au:EPT did not show any sign of degradation after storage for 6 months (Figure S2).[46] Thus, the stability of the three clusters increases in the order Au:OC < Au:PA ≪ Au:EPT. This trend suggests that the Au−C bond and/or interligand attractive force become stronger when the ligand bears a more extended π-conjugated system.

FTIR spectra of Au:OC, Au:PA, and Au:EPT are compared with those of their corresponding ligands in Figure 2. The

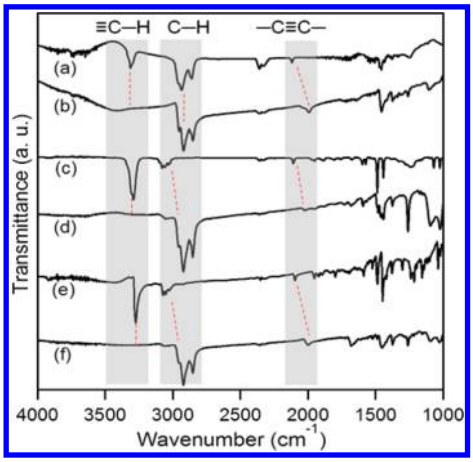

Figure 2. FTIR spectra of (a) OC-H, (b) Au:OC, (c) PA-H, (d) Au:PA, (e) EPT-H, and (f) Au:EPT.

positions and the assignment of the main peaks are summarized in Table 1. Importantly, the alkynyl C−H stretching peaks of

Table 1. FTIR Vibrational Frequencies (cm^{-1}) of Representative Modes of Free Ligands and Those on Au Clusters

sample	≡C−H stretch	−C−H stretch	−C≡C− stretch
OC-H	3313	2846−2973	2121
Au:OC		2832−2965	1995
PA-H	3293	2989−3093	2111
Au:PA		2846−2973	2017
EPT-H	3276	3003−3083	2098
Au:EPT		2843−2962	2008

the free ligands at ∼3300 cm^{-1} are absent in all the clusters, indicating dissociation of the alkynyl C−H bond.[23,29] This result confirms that the alkynyl ligands (RC≡C−) are bonded to the Au clusters (type 1 or 2), ruling out the possibility of bonding in types 3 and 4. The −C≡C− stretching peaks at 2100−2120 cm^{-1} of the free ligands are red-shifted to ∼2000 cm^{-1} in all the clusters. This red shift by ∼110 cm^{-1} indicates weakening of −C≡C− bonds due to electron back-donation from the Au clusters to the π^* orbital of the alkynyl group.[29,37] The peaks at 2850−3100 cm^{-1} are due to C−H stretching of the aliphatic chain or the aromatic ring. The −C═C− stretching of the aromatic ring is also visible at 1500−1600 cm^{-1} in both the free ligands and clusters. These features suggest that interaction between the aromatic ring and Au surface is small and that the alkynyl group is bonded in an upright configuration (type 1) rather than in a flat-lying configuration (type 2). Raman spectra of Au:OC and Au:PA are shown in Figure S3 (Supporting Information).[46] Although the Raman peaks were buried in strong background bands due to PL, we clearly observed a red shift of the −C≡C− stretching peaks upon binding to the Au clusters, consistent with the FTIR results.

RC≡C−Au bonding was formed in the reaction of alkynes with PVP-stabilized Au clusters smaller than 2 nm. What is the fate of terminal hydrogen? A mechanistic understanding of the ligation process is important, because adducts of alkynyl groups on Au NPs have been proposed as key intermediates of Au-catalyzed reactions, including the production of propargylamines via one-pot coupling reactions of aldehydes, alkynes, and amines[42] and diphenylacetylene via Sonogashira cross-coupling of PA-H and iodobenzene.[31] There are two possible scenarios for dissociation of the terminal hydrogen. One is a heterolytic deprotonation, which was theoretically predicted to proceed on the cationic site of Au clusters with the help of base.[31] The other is a homolytic dissociation and subsequent H_2 formation, which was observed in the thiolation of Au clusters.[47] In order to shed light on the question, we first monitored the pH values of the aqueous phase during the reaction of Au:PVP with PA-H. The pH value decreased dramatically from 8.50 to typically ∼3.9. The final pH value is comparable to that (3.32) estimated by assuming that all Au:PVP clusters are fully converted to $Au_{54}(PA)_{26}$.[27] We also monitored the amount of H_2 produced in the ligand exchange by GC analysis. The evolution of H_2 was detected; however, the amount of H_2 was less than 1% of that expected for the complete conversion of Au:PVP into $Au_{54}(PA)_{26}$. These results demonstrate that heterolytic deprotonation of alkyne is a key process in the ligation of the alkynyl group. The deprotonation mechanism is also supported by the fact that the ligation proceeds in the absence of O_2, in sharp contrast to the thiolation of Au:PVP.[48]

Compositions of Magic Clusters. We synthesized $Au_{34}(PA)_{16}$ and $Au_{54}(PA)_{26}$[27] selectively by extracting Au:PVP(**1**) at 283 and 333 K, respectively. Typical yields of $Au_{34}(PA)_{16}$ and $Au_{54}(PA)_{26}$ were ∼20 and ∼70%, respectively. The purity of the samples was confirmed by MALDI mass spectra (Figure 3a,b). In contrast, $Au_{30}(EPT)_{13}$ and $Au_{35}(EPT)_{18}$ could be isolated independently by silica gel column chromatography from Au:EPT, which contained the above species as major species (Figure S4, Supporting Information).[46] In order to obtain larger $Au_n(EPT)_m$, PVP-stabilized Au clusters with an average diameter of 1.4 ± 0.2 nm, Au:PVP(**2**), were prepared (Figure S1, Supporting Information)[46] and used in the synthesis of Au:EPT. The resulting Au:EPT had an average diameter of 1.4 ± 0.2 nm (Figure S5, Supporting Information).[46] Although the average diameters of Au:EPT prepared from Au:PVP(**2**) and Au:PVP(**1**) (Figure 1c) were comparable, mass analysis revealed that the former was mainly comprised of $Au_{41-43}(EPT)_{21-23}$ (Figure S6, Supporting Information).[46] Thus we isolated $Au_{41-43}(EPT)_{21-23}$ from the former sample of Au:EPT by silica gel column chromatography. Figure 3c−e show typical MALDI mass spectra of $Au_n(EPT)_m$ thus isolated. The chemical compositions of these species were determined unambiguously by comparing the mass spectra of Au clusters prepared by PA-H and the *p*-methylated derivative of PA-H.[26] First, the number of ligands was determined by dividing the mass difference between the corresponding cluster with that between CH_3 and H (i.e., 14). Then, the number of Au atoms was determined by dividing the molecular weight difference between the whole cluster and total ligands with the

dx.doi.org/10.1021/ja401798z | J. Am. Chem. Soc. 2013, 135, 9450−9457

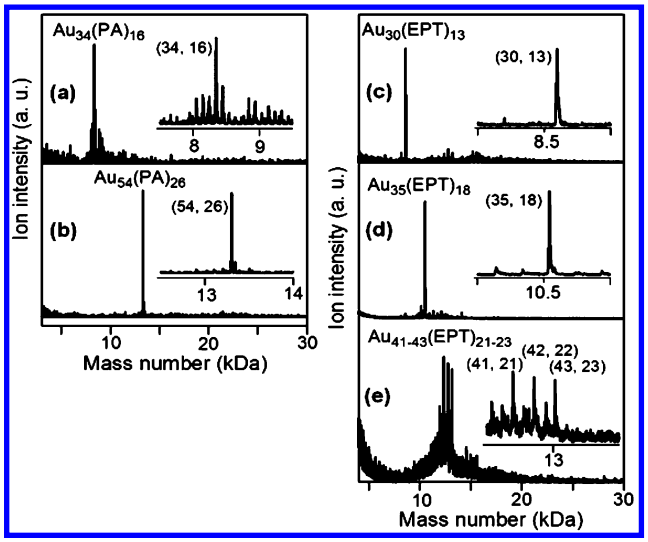

Figure 3. Negative-ion MALDI mass spectra of (a) $Au_{34}(PA)_{16}$, (b) $Au_{54}(PA)_{26}$, (c) $Au_{30}(EPT)_{13}$, (d) $Au_{35}(EPT)_{18}$, and (e) $Au_{41-43}(EPT)_{21-23}$. The inset shows the magnified MALDI mass spectrum for each cluster.

atomic weight of Au atoms (i.e., 197). Such careful mass analysis confirmed that the terminal hydrogen is removed from all of the ligands.[26] This result again excludes the bonding in the intact form (types 3 and 4) and supports the bonding in the dehydrogenated form (type 1 or 2). The Au to ligand ratios of the above isolated clusters are significantly different from those of Au:SR, supporting the different interfacial structures (Figure S7, Supporting Information).[46] The compositions of the isolated magic clusters suggest that the coverage by PA and EPT ligands on the Au surface is approximately 50%. Such high coverage cannot be explained by a flat-lying configuration of the bulky ligands (type 2). We conclude that type 1 is the most plausible model for the bonding motif.

Let us consider the origin of the high stability of the isolated species, even though this is beyond the scope of the present work. It is nontrivial to conclude whether the isolated species are intrinsically stable or not. We cannot rule out the possibility that the isolated clusters are kinetically stabilized during the ligand exchange, since the core sizes for the isolated clusters are similar to those of dominant clusters of Au:PVP(**1**/**2**), such as Au_{24}, Au_{33}, Au_{43}, Au_{58}, and Au_{70} (Figure S1, Supporting Information).[46] The importance of electronic shell closure has been well recognized for bare and ligand-protected Au clusters.[19] According to the electronic shell model for a spherically symmetrical potential field, the electronic shells will be closed with a total number of valence electrons of 2, 8, 18, 20, 34, 40, 58, 70, 92, ...[10,19] The formal numbers of valence electrons in $Au_{34}(PA)_{16}$ and $Au_{41-43}(EPT)_{21-23}$ were calculated to be 18 and 20, respectively, by assuming that the clusters are neutral in the charge state and that each ligand takes one electron from the Au clusters. Hence, we can ascribe the high stability of $Au_{34}(PA)_{16}$ and $Au_{41-43}(EPT)_{21-23}$ to the electronic shell closure. In contrast, the number of valence electrons in $Au_{30}(EPT)_{13}$, $Au_{35}(EPT)_{18}$, and $Au_{54}(PA)_{26}$ are calculated to be 17, 17, and 28, respectively. These numbers do not match those expected for spherical electronic shells. $Au_{30}(EPT)_{13}$ and $Au_{35}(EPT)_{18}$ may have a net charge to make the total number of electrons even. $Au_{54}(PA)_{26}$ possibly adopts a nonspherical geometry wherein 28 valence electrons are filled into the electronic shell.

Photoluminescence of Magic Clusters. Generally, PL from a fluorophore (luminescent organic molecule) is quenched when it is adsorbed on metal clusters/nanoparticles.[49−53] According to Kamat et al.,[49] there are three major deactivation channels for photoexcited fluorophores: (1) energy transfer from the photoexcited fluorophores to the metal clusters, (2) electron transfer from the photoexcited fluorophores to the metal clusters, and (3) interactions between fluorophores. Thus, PL behavior is a sensitive probe of the interaction of Au clusters and fluorophores of alkynyl ligands.

The excitation and emission spectra of the five isolated clusters and free ligands (PA-H and EPT-H) are shown in Figure 4; the complete set of three-dimensional PL spectra is

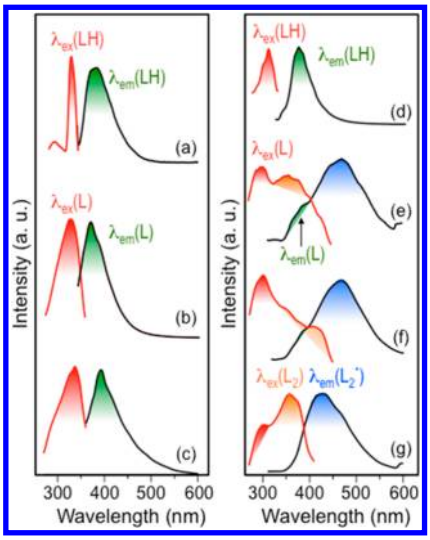

Figure 4. Excitation (red) and emission (black) spectra of (a) PA-H, (b) $Au_{34}(PA)_{16}$, (c) $Au_{54}(PA)_{26}$, (d) EPT-H, (e) $Au_{30}(EPT)_{13}$, (f) $Au_{35}(EPT)_{18}$, and (g) $Au_{41-43}(EPT)_{21-23}$.

summarized in Figure S8 (Supporting Information).[46] The excitation spectra of the five clusters are not similar to their optical absorption spectra (Figure S9, Supporting Information)[46] but rather to those of the corresponding ligands. This result implies that the PL properties observed are mostly governed by those of the ligands on the Au clusters. PA-H was luminescent (λ_{ex} 330 nm, λ_{em} 380 nm) with a quantum yield (Φ) of 2.1×10^{-2} (Figure 4a). $Au_{54}(PA)_{26}$ and $Au_{34}(PA)_{16}$ had similar PL properties (Figure 4b,c) with λ_{em} 390 nm at λ_{ex} 335 nm, although the Φ values were reduced to 2.3×10^{-4} and 3.8×10^{-4}, respectively. The similar PL properties indicate that the photophysical property of PA is not affected significantly upon attachment to the Au cluster and that the phenyl ring is not directly interacting with the Au clusters. This result is consistent with the upright configuration of PA ligands on the Au clusters (type 1).

In contrast, the PL properties of $Au_{30}(EPT)_{13}$, $Au_{35}(EPT)_{18}$, and $Au_{41-43}(EPT)_{21-23}$ were significantly different from those of free EPT-H, which emits λ_{em} 370 nm when excited at λ_{ex} 310 nm with $\Phi = 2.9 \times 10^{-2}$ (Figure 4d). $Au_{30}(EPT)_{13}$, $Au_{35}(EPT)_{18}$, and $Au_{41-43}(EPT)_{21-23}$ showed broad emission (denoted as $\lambda_{em}(L_2^*)$) with peaks at 470, 465, and 425 nm, respectively, when excited at λ_{em} 300 nm. The Φ values were reduced to 2.3×10^{-3}, 1.1×10^{-3}, and 1.1×10^{-3} for $Au_{30}(EPT)_{13}$, $Au_{35}(EPT)_{18}$ and $Au_{41-43}(EPT)_{21-23}$, respectively. These broad emissions (colored blue) were significantly red-shifted from that of EPT-H and assigned to emission from

dx.doi.org/10.1021/ja401798z | J. Am. Chem. Soc. 2013, 135, 9450−9457

the excimer produced by adjacent EPT ligands (Scheme 3). Similar excimer emission was reported for pyrene derivatives

Scheme 3. Possible Excitation and Emission Pathways in Free EPT-H and EPT-Protected Au Clusters

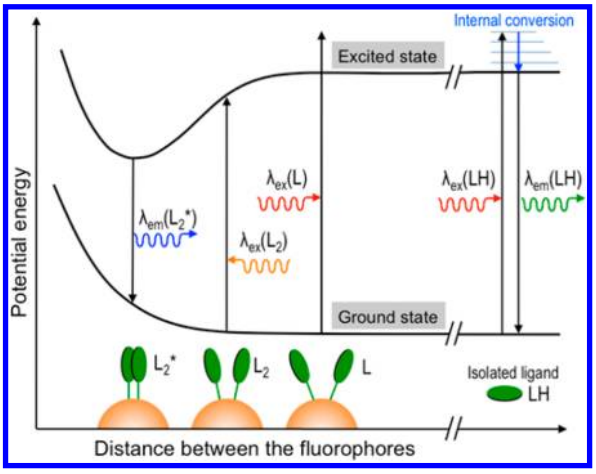

self-assembled on an Au extended surface[54] and on CdSe nanoparticles.[55] However, the present observation is unique, because it is known that excimer emission is not observed from phenanthrene and its derivatives in solution,[56] rather only when phenanthrene rings are forced to overlap through chemical bonds.[57−59] The excimer emission in Figure 4e−g is attributable to close arrangement of the EPT over the Au cluster surface. In the excitation spectra, new bands (colored orange) were clearly observed in addition to those for monomer excitation. These bands (denoted as $\lambda_{ex}(L_2)$) are also associated with the geometrical constraint between adjacent ligands (Scheme 3). The difference in the wavelengths of excimer emission peaks from $Au_{30}(EPT)_{13}$, $Au_{35}(EPT)_{18}$, and $Au_{41-43}(EPT)_{21-23}$ may reflect the difference in the interaction due to the difference in the core size. The observation of excimer emission is additional evidence for the upright configuration of the ligands.

EXAFS Analysis of Magic Clusters. In order to obtain further insights into the structure of Au−C bonds, we measured Au L_3-edge XAFS spectra of three selected clusters, $Au_{34}(PA)_{16}$, $Au_{54}(PA)_{26}$, and $Au_{41-43}(EPT)_{21-23}$ (Figures S10 and S11, Supporting Information).[46] Figure 5 shows the Fourier-transformed EXAFS spectra of $Au_{34}(PA)_{16}$, $Au_{54}(PA)_{26}$, and $Au_{41-43}(EPT)_{21-23}$, together with that for the Au foil as a reference. Table 2 shows the results of curve-fitting analysis by

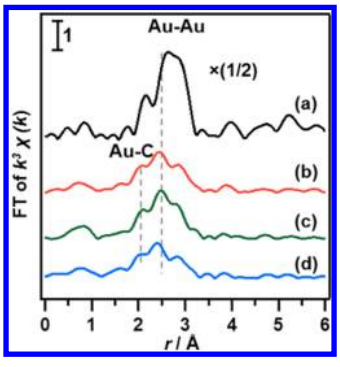

Figure 5. Fourier-transformed EXAFS spectra of (a) Au foil, (b) $Au_{34}(PA)_{16}$, (c) $Au_{54}(PA)_{26}$, and (d) $Au_{41-43}(EPT)_{21-23}$.

assuming an electron mean free path of 0.7 nm. The peaks appearing in the range 1.8−3.2 Å were ascribed to Au−C and Au−Au bonds.

The average coordination number (CN) and bond distance (r) of the Au−Au bond were (CN, r) (4.0, 2.814 Å), (4.2, 2.800 Å), and (4.2, 2.779 Å) for $Au_{34}(PA)_{16}$, $Au_{54}(PA)_{26}$ and $Au_{41-43}(EPT)_{21-23}$, respectively (Table 2). These Au−Au bond distances are slightly smaller than that in bulk Au. The CN values are significantly smaller than those expected for metal clusters smaller than 2 nm; the CN values calculated for cuboctahedral 13- and 55-mers are 5.5 and 7.9, respectively. There are two possible explanations for the underestimation of the average CN values for the Au−Au bonds. The first possibility is associated with the intrinsic structural feature of small-sized clusters in which the Au−Au bond lengths are not uniform.[64] The EXAFS oscillation amplitude is reduced by the presence of nonuniform Au−Au bonds. A second possibility is associated with inelastic electron scattering. Zhao and Montano reported that the electron mean free path (MFP) of clusters increases with decreasing size because of more efficient electron scattering at the surface.[60] In fact, we reported that the Au−Au CN for $Au_{54}(PA)_{26}$ was calculated to be 7.3 ± 1.6 by assuming that the electron MFP is 0.5 nm.[27] In the present work, we systematically investigated the dependence of electron MFP on the CN values for the Au−Au bonds. Figure S12 (Supporting Information)[46] shows that the CN values monotonically increased with a decrease in the MFP values and reached 7.4, 6.1, and 7.4 for $Au_{34}(PA)_{16}$, $Au_{54}(PA)_{26}$, and $Au_{41-43}(EPT)_{21-23}$, respectively, at an MFP of 0.4 nm.

The average CN values of the Au−C bond depend on whether the alkynyl carbon is bonded to an atop site, a bridged site of two atoms, or a hollow site of three atoms of the Au cluster. The average CN values of the Au−C bond are calculated to be 0.5, 0.9−1.1, and 1.4−1.5 for the above three bonding modes, respectively. The experimental CN values of the Au−C bond were 1.1, 1.3, and 1.5 at MFP = 0.7 nm (Table 2) and increased to 2.0, 3.2, and 2.1 at MFP = 0.4 nm (Figure S12, Supporting Information)[46] for $Au_{34}(PA)_{16}$, $Au_{54}(PA)_{26}$, and $Au_{41-43}(EPT)_{21-23}$, respectively. The experimental CN values exclude bonding to an atop site of Au atoms but support bonding to bridged and/or hollow sites. The Au−C bond lengths are in the range 2.2−2.3 Å (Table 2). On the basis of these results, we propose that each alkynyl carbon is bound to two or three Au atoms on the cluster surface. The bonding motif is supported by the theoretical prediction that PA prefers energetically to be bound to the bridged site on Au_{38}[31] and the fcc hollow site on Au(111).[33] The conclusion is also consistent with the DFT result that polyynyl radicals prefer to bind to terraces and steps of an Au surface.[32]

■ CONCLUSION

We investigated the bonding motif between terminal alkynes (OC-H, PA-H, and EPT-H) and Au clusters and their formation process during the ligand exchange of small (<2 nm) Au clusters stabilized by PVP. The structures of the tail groups of the ligands affected the stability of the Au clusters in solution; the stability increased in the order Au:OC < Au:PA ≪ Au:EPT. Vibrational (FTIR and Raman) spectra revealed that terminal hydrogen is lost during the ligand exchange and that the C≡C bond of the alkynyl group (RC≡C−) is weakened upon attachment to the Au clusters. Significant reduction of the pH value of the aqueous phase after the ligand exchange indicated that the ligation of the alkynyl group proceeds via

dx.doi.org/10.1021/ja401798z | J. Am. Chem. Soc. 2013, 135, 9450−9457

Table 2. Results of Curve-Fitting Analysis in the Region of Au−C and Au−Au Bonds[a]

sample	atom[b]	CN[c]	r (Å)[d]	$\Delta\sigma^2$ [e]	R (%)[f]
Au foil	Au	12.5(1.5)	2.884(7)	0.0001(1)	6.2
$Au_{34}(PA)_{16}$	C	1.1(4)	2.224(16)	0.0019(66)	13.5
	Au	4.0(7)	2.814(3)	0.0005(7)	
$Au_{54}(PA)_{26}$	C	1.3(5)	2.231(16)	0.0025(81)	13.8
	Au	4.2(6)	2.800(2)	0.0002(4)	
$Au_{41-43}(EPT)_{21-23}$	C	1.5(5)	2.201(13)	0.0027(52)	14.1
	Au	4.2(8)	2.779(3)	0.0012(11)	

[a]The r fitting range is 1.8−3.2 Å, and the k fitting range is 3.0−13.6 $Å^{-1}$. [b]Bonding atom. [c]Coordination number obtained at an electron mean free path of 0.7 nm. [d]Bond length. [e]Relative Debye−Waller factor: $\Delta\sigma^2 = (\sigma_{sample} - \sigma_{reference})^2$. [f]$R$ factor: $R = (\sum(\chi^{data} - \chi^{fit})^2/\sum(\chi^{data})^2)^{1/2}$.

deprotonation of alkyne. To obtain further detailed information, a series of atomically precise Au clusters, $Au_{34}(PA)_{16}$, $Au_{54}(PA)_{26}$, $Au_{30}(EPT)_{13}$, $Au_{35}(EPT)_{18}$, and $Au_{41-43}(EPT)_{21-23}$, were synthesized. Careful mass analysis confirmed the loss of hydrogen from the ligands and bonding of the alkynyl group on Au. The Au to alkyne ratios exclude the flat-lying orientation of the ligands, and the observation of excimer emission from the EPT ligands confirms the upright configuration. EXAFS analysis suggests that the alkynyl carbon is bound to bridge and/or hollow sites of the Au cluster surfaces.

EXPERIMENTAL SECTION

Chemicals. All reagents were obtained commercially and were used without further purification. Hydrogen tetrachloroaurate tetrahydrate, sodium tetrahydroborate, methanol, toluene, hexane, chloroform, and polyvinylpyrollidine (PVP; K30, average molecular weight 40 kDa), were obtained from Wako Pure Chemical Industries. Phenylacetylene, 1-octyne, 9-ethynyl-phenanthrene, and *trans*-2-[3-(4-*tert*-butylphenyl)-2-methyl-2-propenylidene]malononitrile (DCTB) were purchased from Sigma-Aldrich. Silica gel (mesh size 75−150 μm) was obtained from Wako Pure Chemicals. Milli-Q grade water was used in the present study.

Preparation of PVP Stabilized Au Clusters (1 and 2). Details of the procedure are given in refs 62 and 63. First, an aqueous solution of $HAuCl_4$/PVP (10 mM/0.1 M) was prepared and stirred at 273 K for 30 min. An aqueous solution of $NaBH_4$/PVP (50 mM/0.1 M) was freshly prepared by adding $NaBH_4$ to the aqueous solution of PVP. Then, the thus-prepared solutions of $HAuCl_4$/PVP (15 mL) and $NaBH_4$/PVP (15 mL) were loaded into two syringes and injected by automatically actuated syringe pumps (kdS Scientific, Model No. 780/00E) at a flow rate of 200 mL/h into a micromixer (SIMM-V2, IMM GmbH) kept at 273 K. The hydrosol of the resulting Au:PVP clusters was collected into an ice-cooled Erlenmeyer flask and was stirred for 1 h. Finally, Au:PVP(**1**) clusters were obtained by lyophilizing the deionized dispersion of Au:PVP by ultrafiltration (MWCO = 10 kDa) with water.

An aqueous solution of $HAuCl_4$ (1 mM, 30 mL) was mixed with PVP (K30, 0.6 mmol in monomer unit), and the mixture was stirred for 15 min. Next, Au:PVP clusters were obtained by mixing aqueous solutions of $HAuCl_4$/PVP and $NaBH_4$ (0.1 M, 3 mL) at 273 K. Finally, Au:PVP(**2**) was obtained by lyophilizing the deionized dispersion of the as-prepared Au:PVP clusters by ultrafiltration (MWCO = 10 kDa) with water.

Preparation of Alkyne-Protected Au Clusters. The alkyne -protected Au clusters were prepared by a ligand exchange protocol using water−chloroform biphasic systems. Au:PVP clusters dispersed in water (2.03 mM of Au, 20 mL) were mixed with OC-H, PA-H, or EPT-H in chloroform (406 mM, 10 mL) followed by stirring at 333 K for 2 h. After 2 h, the organic phase turned deep brown and the water became colorless, indicating that complete ligand exchange occurred. The Au:OC, Au:PA, and Au:EPT clusters in the organic phase were collected by evaporating the solvents and repeatedly washing with methanol followed by centrifugation. These clusters are soluble in apolar organic solvents (toluene, chloroform, and dichloromethane) but insoluble in polar organic solvents (methanol and acetone).

Selective Synthesis of $Au_{34}(PA)_{16}$. The synthesis of $Au_{34}(PA)_{16}$ was carried out under conditions similar to those used for $Au_{54}(PA)_{26}$[27] except at a different temperature (283 K) for 10 h, followed by purification as described above.

Silica Gel Column Chromatography. Silica gel (mesh size 75−150 μm) was used as a packing material using hexane/chloroform (1/1) as the initial eluent. Au:EPT samples were loaded onto the column by dissolution in the minimum volume of chloroform. The hexane/chloroform mixture as eluent was then passed continually with a gradual increase in solvent polarity by increasing the chloroform proportion.

Optical Spectroscopy. UV−vis spectra of respective clusters were obtained in water or chloroform as a solvent using a JASCO V-670 spectrophotometer. PL spectra of Au clusters and free ligands were obtained in deaerated chloroform using a JASCO FP-6600 spectrophotometer. Anthracene was used as a standard for the estimation of the quantum yield of the samples.[61]

Transmission Electron Microscopy (TEM). TEM images were recorded using a Philips JEM 2000FX microscope operated at 200 kV. A water dispersion of precursor clusters (**1** and **2**) were drop-casted onto hydrophilic carbon-coated copper grids, and these were then dried in open air for 2 h. Similarly, toluene solutions of Au:OC, Au:PA, and Au:EPT clusters were drop-casted onto hydrophobic carbon-coated copper grids followed by drying in open air for 2 h. These were used in the TEM observations.

Vibrational Spectroscopy. FTIR spectra of all clusters were obtained using a JASCO FT/IR-4200 spectrophotometer with samples prepared as KBr pellets. Raman spectra were recorded on a polychromator (Acton SP300i, 1200 G/mm with SPEC-10 CCD at −65 °C) by excitation of the alkynes at 785 nm (Toptica XTRA, 300 mW) or of the Au clusters at 532 nm (Coherent Compass 315M, 100 mW).

Detection of Terminal Hydrogen. An aqueous phase containing Au:PVP (1 mM of Au, 30 mL) was mixed with a chloroform solution of PA-H (1.5 M, 20 mL) followed by stirring at 333 K for 3 h under an Ar atmosphere. After the reaction, the solution was cooled to room temperature. The pH values of the aqueous phase before and after the reaction were measured using a pH meter (HORIBA, Ltd., 6377-10D), which was calibrated before use. The amount of H_2 contained in the gas phase (3 mL) was monitored using a GC system (Shimadzu GC-8A) with a TCD. A 60/80 molecular sieve 5A column (i.d. 3 mm × 3 m) was used at 40 °C with Ar as a carrier gas.

Matrix-Assisted Laser Desorption Ionization Mass Spectrometry (MALDI MS). Au:PVP samples (2 mg) were dispersed in water (40 μL) in a 1.5 mL centrifuging tube, and DCTB (1 mg) was dissolved in methanol (50 μL) in another tube. Typically, equal amounts of these solutions were mixed in another 1.5 mL centrifuging tube. The mixed solution was cast on a stainless steel plate and dried in the air for over 1 h. In a similar manner, the samples (1 mg) were dissolved in toluene (250 μL) and DCTB (1 mg) was dissolved in methanol (50 μL) in two different tubes. Then three different ratios of these two solutions (1:1, 1:2, and 2:1) were prepared, drop-cast on a stainless steel plate, and dried in the air for over 1 h. MALDI mass spectra of the samples thus prepared were recorded using a time-of-

dx.doi.org/10.1021/ja401798z | J. Am. Chem. Soc. 2013, 135, 9450−9457

flight mass spectrometer (Applied Biosystems, Voyager-DE STR-H) operated with an N_2 laser (337 nm, 3 MHz, <100 mJ). The mass spectra were recorded using an acceleration voltage of 25 kV with delayed extraction mode (delay time 300 ns) in the linear configuration and with both positive and negative detection modes.

X-ray Absorption Spectroscopy. X-ray absorption fine structure (XAFS) measurements were conducted at the BL01B1 beamline at the SPring-8 facility of the Japan Synchrotron Radiation Research Institute. An Si(311) two-crystal monochromator was used for the incident beam for the Au L_3-edge XAFS measurement. XAFS spectra (Figure S10, Supporting Information)[46] were recorded in the transmission mode using ion chambers for the I_0 and I_1 detectors. The solid samples, diluted with boron nitride, were placed between the ion chambers. Energy calibration was carried out using a Cu foil. Data analysis was carried out using the program REX2000 version 2.5.9 (Rigaku Co.). The EXAFS analysis was performed as follows. The χ spectra were extracted by removing the atomic absorption background using a cubic spline and were normalized to the edge height. The k^3-weighted χ spectra (Figure S11, Supporting Information)[46] in the range 3.0−13.6 $Å^{-1}$ were Fourier-transformed (FT) into r space. Curve-fitting analysis was performed for the Au−C and Au−Au bonds appearing at 1.8−3.2 Å. A passive electron factor (S_0^2) of 1 was used in this study. The phase and amplitude functions were extracted from AuC (space group $P\bar{6}m2$, ICSD No. 169406) and Au metal (space group $Fm\bar{3}m$, ICSD No. #44362) by calculation using FEFF8.[65]

■ ASSOCIATED CONTENT

Supporting Information

Figures giving additional TEM images, UV−vis spectra, MALDI mass spectra, EXAFS spectra, and PL spectra. This material is available free of charge via the Internet at http://pubs.acs.org.

■ AUTHOR INFORMATION

Corresponding Author

*E-mail for T.T.: tsukuda@chem.s.u-tokyo.ac.jp.

Notes

The authors declare no competing financial interest.

■ ACKNOWLEDGMENTS

This research was financially supported by the Funding Program for Next Generation World-leading Researchers (NEXT Program, GR-003) and MEXT program "Elements Strategy Initiative to Form Core Research Center" (since 2012), MEXT Ministry of Education Culture, Sports, Science and Technology of Japan. The XAFS measurements at the SPring-8 facility were carried out with the approval of the Japan Synchrotron Radiation Research Institute (JASRI) (Proposal No. 2012B1074).

■ REFERENCES

(1) Schmid, G. *Chem. Soc. Rev.* **2008**, *37*, 1909.
(2) Whetten, R. L.; Khoury, J. T.; Alvarez, M. M.; Murthy, S.; Vezmar, I.; Wang, Z. L.; Stephens, P. W.; Cleveland, C. L.; Luedtke, W. D.; Landman, U. *Adv. Mater.* **1996**, *8*, 428.
(3) Templeton, A. C.; Wuelfing, W. P.; Murray, R. W. *Acc. Chem. Res.* **2000**, *33*, 27.
(4) Aikens, C. M. *J. Phys. Chem. Lett.* **2011**, *2*, 99.
(5) Maity, P.; Xie, S.; Yamauchi, M.; Tsukuda, T. *Nanoscale* **2012**, *4*, 4027.
(6) Pei, Y.; Zeng, X. C. *Nanoscale* **2012**, *4*, 4054.
(7) Zheng, J.; Zhou, C.; Yu, M. X.; Liu, J. B. *Nanoscale* **2012**, *4*, 4073.
(8) Qian, H.; Zhu, M. Z.; Wu, Z. K.; Jin, R. *Acc. Chem. Res.* **2012**, *45*, 1470.
(9) Tsukuda, T. *Bull. Chem. Soc. Jpn.* **2012**, *85*, 151.
(10) Häkkinen, H. *Nat. Chem.* **2012**, *4*, 443.
(11) Briant, C. E.; Theobald, B. R. C.; White, J. W.; Bell, L. K.; Mingos, D. M. P. *J. Chem. Soc., Chem. Commun.* **1981**, 201.
(12) Bos, W.; Kanters, R. P. F.; van Halen, C. J.; Bosman, W. P.; Behm, H.; Smits, J. M. M.; Beurskens, P. T.; Bour, J. J.; Pignolet, L. H. *J. Organomet. Chem.* **1986**, *307*, 385.
(13) Teo, B. K.; Shi, X.; Zhang, H. *J. Am. Chem. Soc.* **1992**, *114*, 2743.
(14) Jadzinsky, P. D.; Calero, G.; Ackerson, C. J.; Bushnell, D. A.; Kornberg, R. D. *Science* **2007**, *318*, 430.
(15) Nunokawa, K.; Onaka, S.; Ito, M.; Horibe, M.; Yonezawa, T.; Nishihara, H.; Ozeki, T.; Chiba, H.; Watase, S.; Nakamoto, M. *J. Organomet. Chem.* **2006**, *691*, 638.
(16) Shichibu, Y.; Negishi, Y.; Watanabe, T.; Chaki, N. K.; Kawaguchi, H.; Tsukuda, T. *J. Phys. Chem. C* **2007**, *111*, 7845.
(17) Zeng, C.; Qian, H.; Li, T.; Li, G.; Rosi, N. L.; Yoon, B.; Barnett, R. N.; Whetten, R. L.; Landman, U.; Jin, R. *Angew. Chem., Int. Ed.* **2012**, *51*, 13114.
(18) Nishigaki, J.; Tsunoyama, R.; Tsunoyama, H.; Ichikuni, N.; Yamazoe, S.; Negishi, Y.; Ito, M.; Matsuo, T.; Tamao, K.; Tsukuda, T. *J. Am. Chem. Soc.* **2012**, *134*, 14295.
(19) Walter, M.; Akola, J.; Lopez-Acevedo, O.; Jadzinsky, P. D.; Calero, G.; Ackerson, C. J.; Whetten, R. L.; Grönbeck, H.; Häkkinen, H. *Proc. Natl. Acad. Sci. U.S.A.* **2008**, *105*, 9157.
(20) Daniel, M.-C.; Astruc, D. *Chem. Rev.* **2004**, *104*, 293.
(21) Jiang, D.; Sumpter, B. G.; Dai, S. *J. Am. Chem. Soc.* **2006**, *128*, 6030.
(22) Mirkhalaf, F.; Paprotny, J.; Schiffrin, D. J. *J. Am. Chem. Soc.* **2006**, *128*, 7400.
(23) Zhang, S.; Chandra, K. L.; Gorman, C. B. *J. Am. Chem. Soc.* **2007**, *129*, 4876.
(24) Kumar, V. K. R.; Gopidas, K. R. *Chem. Asian J.* **2010**, *5*, 887.
(25) Laurentius, L.; Stoyanov, S. R.; Gusarov, S.; Kovalenko, A.; Du, R.; Lopinski, G. P.; McDermott, M. T. *ACS Nano* **2011**, *5*, 4219.
(26) Maity, P.; Tsunoyama, H.; Yamauchi, M.; Xie, S.; Tsukuda, T. *J. Am. Chem. Soc.* **2011**, *133*, 20123.
(27) Maity, P.; Wakabayashi, T.; Ichikuni, N.; Tsunoyama, H.; Xie, S.; Yamauchi, M.; Tsukuda, T. *Chem. Commun.* **2012**, *48*, 6085.
(28) Hong, W.; Li, H.; Liu, S.-X.; Fu, Y.; Li, J.; Kaliginedi, V.; Decurtins, S.; Wandlowski, T. *J. Am. Chem. Soc.* **2012**, *134*, 19425.
(29) Kang, X.; Zuckerman, N. B.; Konopelski, J. P.; Chen, S. *Angew. Chem., Int. Ed.* **2010**, *49*, 9496.
(30) Joo, S.-W.; Kim, K. *J. Raman Spectrosc.* **2004**, *35*, 549.
(31) Boronat, M.; Combita, D.; Concepción, P.; Corma, A.; García, H.; Juárez, R.; Laursen, S.; López-Castro, J. d. D. *J. Phys. Chem. C* **2012**, *116*, 24855.
(32) Nykänen, L.; Häkkinen, H.; Honkala, K. *Carbon* **2012**, *50*, 2752.
(33) Ford, M. J.; Hoft, R. C.; McDonagh, A. *J. Phys. Chem. B* **2005**, *109*, 20387.
(34) Patterson, M. L.; Weaver, M. J. *J. Phys. Chem.* **1985**, *89*, 5046.
(35) Feilchenfeld, H.; Weaver, M. J. *J. Phys. Chem.* **1989**, *93*, 4276.
(36) Li, Q.; Han, C.; Fuentes-Cabrera, M.; Terrones, H.; Sumpter, B. G.; Lu, W.; Bernholc, J.; Yi, J.; Gai, Z.; Baddorf, A. P.; Maksymovych, P.; Pan, M. *ACS Nano* **2012**, *6*, 9267.
(37) Chen, W.; Zuckerman, N. B.; Kang, X.; Ghosh, D.; Konopelski, J. P.; Chen, S. *J. Phys. Chem. C* **2010**, *114*, 18146.
(38) Kang, X.; Zuckerman, N. B.; Konopelski, J. P.; Chen, S. *J. Am. Chem. Soc.* **2012**, *134*, 1412.
(39) Lopez-Sanchez, J. A.; Lennon, D. *Appl. Catal., A* **2005**, *291*, 230.
(40) Nikolaev, S. A.; Permyakov, N. A.; Smirnov, V. V.; Vasil'kov, A. Y.; Lanin, S. N. *Kinet. Catal.* **2010**, *51*, 288.
(41) Stratakis, M.; Garcia, H. *Chem. Rev.* **2012**, *112*, 4469.
(42) Kidwai, M.; Bansel, V.; Kumar, A.; Mozumdar, S. *Green Chem.* **2007**, *9*, 742.
(43) Corma, A.; Leyva-Pérez, A.; Sabater, M. J. *Chem. Rev.* **2011**, *111*, 1657.
(44) Oliver-Meseguer, J.; Cabrero-Antonino, J. R.; Domínguez, I.; Leyva-Pérez, A.; Corma, A. *Science* **2012**, *338*, 1452.
(45) Brust, M.; Walker, M.; Bethell, D.; Schiffrin, D. J.; Whyman, R. *J. Chem. Soc., Chem. Commun.* **1994**, 801.
(46) See the Supporting Information.

(47) Matthiesen, J. E.; Jose, D.; Sorensen, C. M.; Klabunde, K. J. *J. Am. Chem. Soc.* **2012**, *134*, 9376.
(48) Tsunoyama, H.; Nickut, P.; Negishi, Y.; Al-Shamery, K.; Matsumoto, Y.; Tsukuda, T. *J. Phys. Chem. C* **2007**, *111*, 4153.
(49) Thomas, K. G.; Kamat, K. V. *Acc. Chem. Res.* **2003**, *36*, 888.
(50) Ipe, B. I.; Thomas, K. G. *J. Phys. Chem. B* **2004**, *108*, 13265.
(51) Barazzouk, S.; Kamat, P. V.; Hotchandani, S. *J. Phys. Chem. B* **2005**, *109*, 716.
(52) Nerambourg, N.; Werts, M. H. V.; Charlot, M.; Blanchard-Desce, M. *Langmuir* **2007**, *23*, 5563.
(53) Devadas, M. S.; Kwak, K.; Park, J.-W.; Choi, J.-H.; Jun, C.-H.; Sinn, E.; Ramakrishna, G.; Lee, D. *J. Phys. Chem. Lett.* **2010**, *1*, 1497.
(54) Nakamura, M.; Saito, N.; Takayama, K.; Kumamoto, S.; Yamada, K. *Chem. Lett.* **2007**, *36*, 602.
(55) Agudelo-Morales, C. E.; Galian, R. E.; Pérez-Prieto, J. *Anal. Chem.* **2012**, *84*, 8083.
(56) Chandross, E. A.; Thomas, H. T. *J. Am. Chem. Soc.* **1972**, *94*, 2421.
(57) Nakamura, Y.; Tsuihiji, T.; Mita, T.; Minowa, T.; Tobita, S.; Shizuka, H.; Nishimura, J. *J. Am. Chem. Soc.* **1996**, *118*, 1006.
(58) Nakamura, Y.; Fujii, T.; Nakamura, J. *Chem. Lett.* **2001**, *30*, 970.
(59) Nakamura, Y.; Yamazaki, T.; Nakamura, J. *Org. Lett.* **2005**, *7*, 3259.
(60) Frenkel, A. I.; Yevick, A.; Cooper, C.; Vasic, R. *Annu. Rev. Anal. Chem.* **2011**, *4*, 23.
(61) Zhao, J.; Montano, P. A. *Phys. Rev. B* **1989**, *40*, 3401.
(62) Tsunoyama, H.; Sakurai, H.; Ichikuni, N.; Negishi, Y.; Tsukuda, T. *Langmuir* **2004**, *20*, 11293.
(63) Tsunoyama, H.; Ichikuni, N.; Tsukuda, T. *Langmuir* **2008**, *24*, 11327.
(64) Melhuish, W. H. *J. Phys. Chem.* **1961**, *65*, 229.
(65) Ankudinov, A. L.; Ravel, B.; Rehr, J. J.; Conradson, S. D. *Phys. Rev. B* **1998**, *58*, 7565.